

Entanglement distribution with wavevector-multiplexed quantum memory

Michał Lipka,^{1,2} Mateusz Mazelanik,^{1,2} and Michał Parniak^{1,3,*}

¹*Centre for Quantum Optical Technologies, Centre of New Technologies,
University of Warsaw, Banacha 2c, 02-097 Warsaw, Poland*

²*Faculty of Physics, University of Warsaw, Pasteura 5, 02-093 Warsaw, Poland*

³*Niels Bohr Institute, University of Copenhagen,
Blegdamsvej 17, DK-2100 Copenhagen, Denmark*

Feasible distribution of quantum entanglement over long distances remains a fundamental step towards quantum secure communication and quantum network implementations. Quantum repeater nodes based on quantum memories promise to overcome exponential signal decay inherent to optical implementations of quantum communication. While performance of current quantum memories hinders their practical application, multimode solutions with multiplexing can offer tremendous increase in entanglement distribution rates. We propose to use a wavevector-multiplexed atomic quantum memory (WV-MUX-QM) as a fundamental block of a multiplexed quantum repeater architecture. We show the WV-MUX-QM platform to provide quasi-deterministic entanglement generation over extended distances, mitigating the fundamental issue of optical loss even with currently available quantum memory devices, and exceeding performance of repeaterless solutions as well as other repeater-based protocols such as temporal multiplexing. We establish the entangled-bit (ebit) rate per number of employed nodes as a practical figure of merit reflecting the cost-efficiency of larger inter-node distances.

I. INTRODUCTION

Entanglement is an essential resource for the most promising quantum information protocols [1, 2] enabling, among others, secure quantum communication [3–5]. The optical implementations of such protocols face the exponential transmission losses inherent to photonic systems and greatly limiting the feasible distance at which high fidelity entangled states can be distributed. To overcome this obstacle, noise-tolerant quantum repeaters have been proposed for entanglement connection and purification over shorter elementary lengths [6].

Experimentally promising quantum repeater architectures involve linear optics, quantum memories and single-photon detection [7, 8]; however, currently available memory lifetimes as well as retrieval and single-photon detection efficiencies limit the feasibility of such repeaters at practical distances of a few hundred km [9, 10]. Multimode architectures have been proposed as solutions to this problem [11–13], which lead to an ongoing effort in experimental realizations of such systems, especially involving multiplexing capabilities. While an M -mode platform in parallel operation increases the entanglement distribution rate M -fold, multiplexing may lead to $\mathcal{O}(M^{2N})$ -fold increase with N denoting the number of repeater nodes [11]. Hitherto multimode systems demonstrated in the context of quantum repeaters involved at most tens of modes [14–19] and mainly focused on temporal multiplexing. As an alternative to temporal, spectral or spatial micro-ensemble modes [20], a highly-multimode wavevector multiplexed quantum memory (WV-MUX-QM) has been recently demonstrated [21]

along with flexible in-memory processing capabilities [22–24].

Here we evaluate the feasibility of previously-demonstrated WV-MUX-QM, which was based on a high-optical-depth cold atomic ensemble, as a quantum repeater platform. Remaining in the constraints of current technology, we propose a multiplexing protocol combining experimentally demonstrated components to provide quasi-deterministic entanglement generation over 150 km.

We analyse the performance of the novel platform in the recently proposed semihierarchical quantum repeater architecture [25] as well as an ahierarchical architecture and compare the performance of wavevector multiplexing with state-of-the art temporal multimode and long-lifetime single-mode platforms. Finally, we identify the fundamental limitations of the WV-MUX-QM platform. Our results are particularly significant in the light of recent advances and effort in developing practically feasible multi-mode quantum communication systems employing multicore fibres [26, 27] or free-space transmission [28].

Quantum repeaters – DLCZ protocol

As proposed by Duan, Lukin, Cirac and Zoller (DLCZ) in their seminal paper [29], atomic ensemble-based quantum memories and linear optical operations combined with single-photon detection can be employed to transfer entanglement between distant parties. In a simple scenario of the DLCZ protocol, two parties – Alice (A) and Bob (B) – are separated by a distance L and would like to share a high-fidelity entangled photonic state for further use in quantum communication protocols such as Quantum Key Distribution (QKD). If the optical losses are too large over the distance L , we can ima-

* parniak@nbi.ku.dk

gine N equidistant parties separated by $L_0 = L/(N-1)$. Each party (A_i) has two atomic ensembles and independently generates entanglement between one of the ensembles and one of her neighbours (A_{i-1}, A_{i+1}). Then, hierarchically, the parties read their two ensembles and, conditioned on a successful detection of a single read-out photon, extend the entanglement to their neighbours ($A_{i-1} \leftrightarrow A_i \leftrightarrow A_{i+1} \rightarrow A_{i-1} \leftrightarrow A_{i+1}$).

The DLCZ protocol, being based on single-photon interference, requires sub-wavelength phase stability over tens-of-km inter-node distances L_0 , limiting its practical feasibility. Furthermore, in a DLCZ-based network the distributed entangled state contains a vacuum component which grows with every entanglement swapping stage. As a solution to those issues, two-photon interference-based protocols have been proposed [8, 30] and experimentally demonstrated [7, 10]. In this work we build on the two-photon protocols [8, 30] inherently robust to optical phase stability. In particular, while we design the entanglement generation (ENG) scheme specifically for WV-MUX-QM platform, the entanglement connection (ENC), which takes place after multiplexing (MUX), remains the same as in standard two-photon protocols.

The basic idea of two-photon protocols is to employ polarization entangled pairs of photons instead of occupation number entangled state with a single photon. In a basic scenario the i -th node A_i has a pair of memories $A_i^{(H,L)}, A_i^{(V,L)}$ for ENG with A_{i-1} and another pair $A_i^{(H,R)}, A_i^{(V,R)}$ for A_{i+1} . Polarization of photons emitted from the memories is transformed so that the superscripts H and V correspond to horizontal and vertical polarization of the photons, respectively. Similarly to the DLCZ protocol, photons from A_i and A_{i+1} are sent to the midway station and interfered on a beamsplitter; however, now the interference and single-photon detection is separate for each polarization. For ENC both H and V memories are readout and the state of the distant pairs of memories is projected onto a maximally entangled Bell state by measuring the read-out photons and post-selecting outcomes.

II. RESULTS

Wavevector-multiplexed quantum repeater

Multimode quantum memory

The WV-MUX-QM platform is based on an atomic quantum memory. For specificity we shall consider rubidium-87 atoms [21] cooled in a magneto-optical trap (MOT) via polarization gradient cooling and trapped in a dipole trap [31] reaching temperatures of $1 \mu\text{K}$. The memory operates via a light-atom interface based on an off-resonant spontaneous Raman scattering. A lambda configuration of atomic levels is involved, as depicted in the inset of Fig. 1. Importantly, the selected atomic

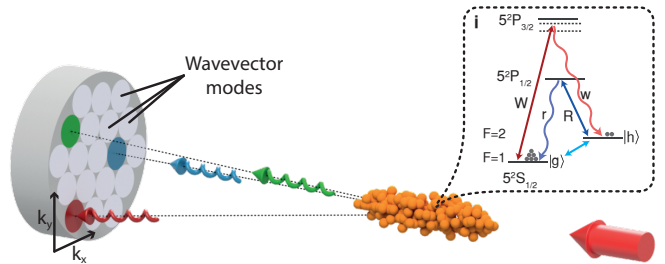


Figure 1. With wavevector multiplexing, each mode of such an atomic memory corresponds to a different angle of emission (or wavevector) of write-out (read-out) photons. **i** Atomic levels in a lambda configuration for a light-atom interface to the wavevector multiplexed quantum memory based on cold rubidium-87 atoms. W - write beam, R - read beam, w - write-out photon, r - read-out photon. For technical reasons our experiments presented in [21] used different atomic transitions for writing and reading.

transitions should be clock transitions robust to external magnetic fields [32]. The atoms are initially prepared in the $|g\rangle$ level. A strong write (W) beam off-resonant with $|g\rangle \rightarrow |e\rangle$ transition generates a two-mode squeezed state of scattered write-out (Stokes) photons and collective atomic excitations (spin-waves, coherence between $|g\rangle$ and $|h\rangle$ levels). Let us denote by $\hat{a}_{\mathbf{k}_w}^\dagger$ the creation operator for write-out photon with a wavevector \mathbf{k}_w determining the scattering angle and the memory mode, as depicted in Fig. 1. Denoting creation operator for a single spin-wave with wavevector \mathbf{K} by $\hat{S}_{\mathbf{K}}^\dagger$, the generated state in a single pair of memory and photonic modes is given by:

$$|\psi\rangle = \sum_{j=0} (\sqrt{\chi} \hat{S}_{\mathbf{K}}^\dagger \hat{a}_{\mathbf{k}_w}^\dagger)^j |\text{vac}\rangle, \quad (1)$$

where χ gives the probability of generating a single pair of photon-spin-wave excitations. After a programmable delay, the spin-waves can be converted to read-out photons with a strong resonant read (R) beam $\hat{S}_{\mathbf{K}}^\dagger \rightarrow \hat{a}_{\mathbf{k}_r}^\dagger$.

Write and read processes conserve momentum and energy which results in correlated momenta or wavevectors (or scattering angles) of write-out and read-out photons. While, in general, phase-matching conditions must be taken into consideration, the most versatile write/read beams configuration employs counter-propagating beams at angle of around 2° to the longitudinal axis of MOT [21]. Importantly, with such a choice of write and read beams' wavevectors, the write-out photon at \mathbf{k}_w heralds further read-out to result in a read-out photon at $\mathbf{k}_r \approx -\mathbf{k}_w$, which is fundamental for wavevector multiplexing.

Entanglement distribution

An ahierarchical quantum repeater architecture has been depicted in Fig. 2a. Each node contains two

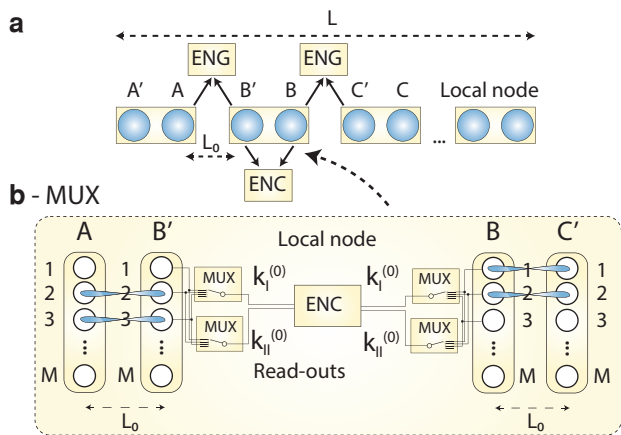


Figure 2. **a** Entanglement distribution with an ahierarchical quantum repeater architecture and employing atomic wavevector multiplexed quantum memories (WV-MUX-QM). Each node consists of two WV-MUX-QM (e.g. A', A). Intermediate nodes are located L_0 apart and send the write-out photons generated in one of their atomic ensembles to a mid-way station in order to generate entanglement (ENG) between the distant ensembles (e.g. A and B'). **b** Multiplexing idea – to entangle ensembles A and C' in entanglement connection stage (ENC) after successful ENG between A & B' and B & C' , the read-out photons from B and B' are multiplexed to pre-selected modes $\mathbf{k}_I^{(0)}$, $\mathbf{k}_{II}^{(0)}$ with a reconfigurable MUX and using the which-mode information from ENG stages.

WV-MUX-QMs. Distant memories perform entanglement generation (ENG) by sending write-out photons to a central mid-way station. To distribute the entanglement, memories are read at each node and the read-out photonic modes are multiplexed to pre-selected modes, as depicted in Fig. 2b, to further undergo entanglement connection (ENC).

Entanglement generation (ENG)

The first operation in a quantum repeater link is the generation of entanglement (ENG) between each pair of quantum memories separated by an elementary distance $L_0 = L/(N-1)$. The memories probabilistically generate entangled pairs of atomic excitations and single-photons across M modes of their ensembles. The generated write-out photons are sent to a central mid-way station (CMS) via multimode channels. We note here that there is no inter-mode phase stability requirement, rendering either free space or multimode fibres a viable multimode channel. On the other hand, a space-to-time conversion [33] could be used to map the wavevector modes to time bins and thus enabling use of single-mode channels for ENG. The photons generated in each ensemble are divided by their emission angles into two groups with imposed orthogonal polarizations – vertical (V) and horizontal (H), as depicted in Fig. 3a. Before transmission, the two groups are super-imposed on each-other to ensure that each pair

of H, V modes is transmitted through a single channel acquiring the same optical phase or a deterministic phase difference.

Let us consider two ensembles A, B' located in separate nodes. Horizontal (vertical) polarization from A is superimposed onto vertical (horizontal) polarization from B' , erasing the which-node information and resulting in four regions containing M modes each. The regions \mathbf{I}_\pm (\mathbf{II}_\pm) observe V (H) polarization from B' and H (V) polarization from A . A single-photon sensitive camera [34] observes the regions and registers coincidences between any of modes in \mathbf{I}_\pm (\mathbf{k}_I) and any of modes in \mathbf{II}_\pm (\mathbf{k}_{II}), which projects the state of atomic ensembles A, B' onto:

$$|\psi_{\text{ENG}}^{A,B'}\rangle = \frac{1}{\sqrt{2}}(\hat{S}_{A,H,\mathbf{k}_I}^\dagger + \exp(i\phi)\hat{S}_{B',V,\mathbf{k}_I}^\dagger) \quad (2)$$

$$\times (\hat{S}_{A,V,\mathbf{k}_{II}}^\dagger + \exp(i\phi)\hat{S}_{B',H,\mathbf{k}_{II}}^\dagger)|\text{vac}\rangle, \quad (3)$$

where ϕ gives the phase difference between optical paths from A and B' to the midway CMS i.e. over distance $L_0/2$, and $\hat{S}_{X,P,\mathbf{k}}^\dagger$ is the creation operator for a spin-wave in ensemble X , in mode \mathbf{k} , with the corresponding read-out photon P -polarized. Here and henceforth the modes are indexed by the wavevector of the write-out photon \mathbf{k} which implicitly corresponds to a spin-wave in mode \mathbf{K} , which upon readout generates a read-out photon in mode $-\mathbf{k}$. We note here that since the coincidence can occur between any two modes there is M^2 possibilities, in contrast to parallel scheme which attempts ENG only between the j -th mode from A and j -th mode from B' .

The excitation number (DLCZ-type) entanglement present in $|\psi_{\text{ENG}}^{A,B'}\rangle$ will be further converted to polarization entanglement during entanglement connection (ENC) stage which also projects the state onto a subspace containing one excitation per node.

Let us consider the probability of a successful ENG between A and B' with multiplexing and by utilizing the memory modes in parallel. If we denote the total probability of emitting two photons, transmission and correct measurement outcome by p_1 , then with M modes the total probability of successful ENG in any pair of modes in *parallel* operation would read

$$p_g^{(\text{parallel})} = 1 - (1 - p_1)^M. \quad (4)$$

With multiplexing we harness the multi-mode single-photon detection at CMS to provide the which-mode information about photons from each memory, which further enables reconfiguration of a M -to-1 switch at the memories' outputs. This way, we can entangle each of M modes from A with each of M modes from B' , effectively enhancing the probability of entanglement generation

$$p_g = 1 - (1 - p_1)^{M^2}. \quad (5)$$

We note that this probability is equivalent to the parallel case with M^2 modes.

Importantly, the single-mode ENG probability p_1 involves a fundamental transmission loss which can be mitigated by M^2 scaling in p_g . Wavevector multiplexed

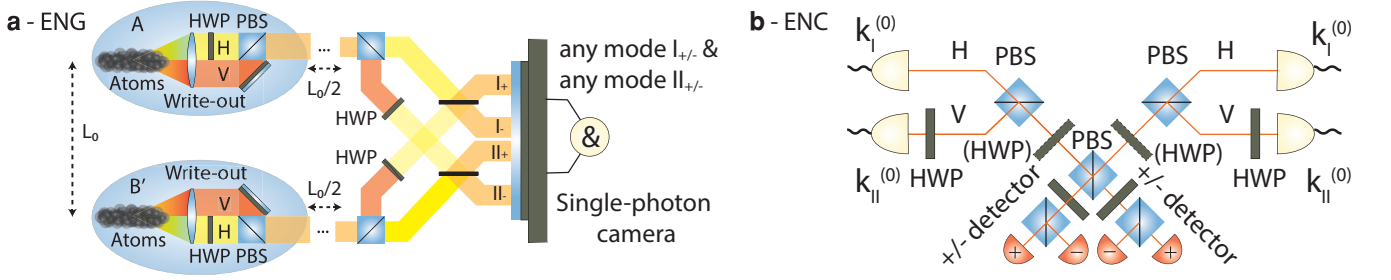


Figure 3. **a** The WV-MUX-QM involves an atomic ensemble optically interfaced via spontaneous Raman scattering which generates pairs of a write-out photon and a collective atomic-excitation – a spin-wave. In the far-field of the atomic ensemble the wavevector (angular) modes of write-out photons are divided into two groups with imposed horizontal (H) or vertical (V) polarization, and the groups are super-imposed. Entanglement generation (ENG) between two distant WV-MUX-QM memories – A' and B involves multimode transmission of write-out photons to a midway station. Due to spatially resolved single-photon detection (single-photon camera), any of M modes from A' can be entangled with any of M modes from B giving M^2 possibilities and facilitating quasi-deterministic ENG even with substantial losses. The ENG is heralded by a detection of a coincidence between a photon in regions I_{\pm} and in regions II_{\pm} . **b** Entanglement connection (ENC) stage takes place at a local node. The memories are read and read-out photons are multiplexed to pre-selected optical modes $\mathbf{k}_I^{(0)}$, $\mathbf{k}_{II}^{(0)}$. Upon a coincidence detection between different \pm detectors, the optical setup projects the spin-wave state of ensembles A and C' onto a maximally entangled Bell state. PBS - polarizing beamsplitter, HWP - half-wave plate set at 45° , (HWP) - optional HWP for first-stage ENC.

quantum memories can achieve around 5×10^3 modes, making the entanglement generation quasi-deterministic, even with significant optical attenuation at large elementary distances L_0 .

Entanglement connection (ENC)

Let us assume that ENGs have been successful between A and B' , and between B and C' , to form a state $|\psi_{\text{ENG}}^{A,B'}\rangle \otimes |\psi_{\text{ENG}}^{B,C'}\rangle$ involving modes \mathbf{k}_I , \mathbf{k}_{II} , \mathbf{k}_{III} and \mathbf{k}_{IV} . Ensembles B and B' are at the same node. We wish to carry ENC with B , B' so that A and C' share an entangled state. Let us for the moment postpone the discussion of the multiplexing stage and assume that read-out photons from B and B' occupying superpositions of \mathbf{k}_I , \mathbf{k}_{II} and \mathbf{k}_{III} , \mathbf{k}_{IV} modes, respectively, arrive at the ENC segment in pre-selected photonic modes. For entanglement connection (ENC) a two-photon interference is observed between the read-out photons with single-photon detectors, as depicted in Fig. 3b. Once a coincidence with one photon per each depicted \pm detector is observed, the ENC succeeds with an output state depending on the coincidence detectors signs (\pm, \pm) . For example $(+, +)$ gives $(|HV\rangle_{A,C'} + |VH\rangle_{A,C'})/\sqrt{2} \equiv (\hat{S}_{A,H,\mathbf{k}_I}^\dagger \hat{S}_{C',V,\mathbf{k}_{IV}}^\dagger + \hat{S}_{A,V,\mathbf{k}_{II}}^\dagger \hat{S}_{C',H,\mathbf{k}_{III}}^\dagger)/\sqrt{2}$, while $(+, -)$ leads to $(|HH\rangle_{A,C'} + |VV\rangle_{A,C'})/\sqrt{2}$. The output state can be corrected with a bit-flip operation so that ENC always yields the same Bell state. While first-stage ENC (fENC) taking place just after ENG requires additional half-wave plates in the setup, further ENCs proceed without the second polarization rotation, as depicted in Fig. 3b, and require a phase-flip correction instead of a bit-flip [35].

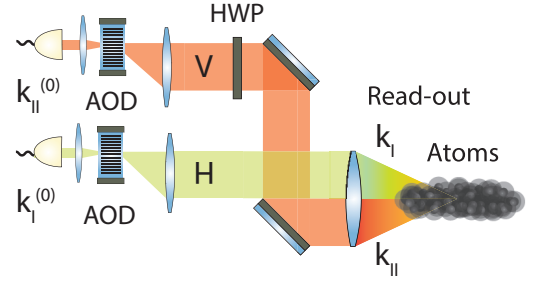


Figure 4. Wavevector mode multiplexing with acousto-optical deflectors (AOD). The which-mode information acquired during multimode entanglement generation predicts the emission of a read-out photon at wavevector modes \mathbf{k}_I or \mathbf{k}_{II} , with the two modes located in separate halves of the emission cone. The cone is split in the far-field of the atomic cloud. Each half is multiplexed separately. By imaging the atomic cloud onto the AOD we can shift the wavevector of the read-out photon from \mathbf{k}_I (\mathbf{k}_{II}) to the desired mode $\mathbf{k}_I^{(0)}$ ($\mathbf{k}_{II}^{(0)}$) which can be coupled to a single-mode fibre and routed to a single-mode entanglement connection setup.

Multiplexing (MUX)

A critical step in the new protocol is multiplexing (MUX) the arbitrary modes in $|\psi_{\text{ENG}}\rangle$ to a pair of canonical pre-selected modes, which enables two-photon interference between the read-out photons, crucial for robust entanglement swapping [8, 35]. Several strategies may be employed to implement the MUX stage. Importantly, spatially-resolved detection involved in the new protocol at the ENG station provides the required which-mode

($\mathbf{k}_I, \mathbf{k}_{II}$) information. One idea may be to interface the memory with two read beams at angles which are reconfigured via acousto-optical deflectors (AOD) to facilitate the read-out at pre-select modes $\mathbf{k}_I^{(0)}, \mathbf{k}_{II}^{(0)}$ [36].

Another MUX method which may yield close to 100% efficiency would be to use fast acousto-optical deflectors (AOD) placed in the near-field of the atomic cloud, to directly adjust the wavevector (angle) of the read-out photons to match $\mathbf{k}_I^{(0)}$ and $\mathbf{k}_{II}^{(0)}$. The idea has been depicted in Fig. 4. Importantly, \mathbf{k}_I and \mathbf{k}_{II} always lay in different (H, V) parts of the emission cone and thus can be separated in the far-field and directed to two different AODs. Each AOD modulates the read-out with only a single frequency reconfigured to match the difference between the actual modes ($\mathbf{k}_I, \mathbf{k}_{II}$) and the target modes ($\mathbf{k}_I^{(0)}, \mathbf{k}_{II}^{(0)}$).

Alternatively, fast digital micromirror devices (DMDs) approaching μs response times could be used in place of AODs offering even broader possibilities [37].

A more flexible technique could involve an in-memory MUX on the stored spin-waves. The required technique – ac-Stark spin-wave modulation – has been demonstrated [22–24] in implementations of single-spin-wave inter-mode operations and spin-wave wavevector (\mathbf{K} -space) displacements. In this approach, the which-mode information is used to prepare a spin-wave \mathbf{K} -space displacement operation which changes the wavevectors of stored spin-waves to make the read-out photons match the pre-selected modes $\mathbf{k}_I^{(0)}, \mathbf{k}_{II}^{(0)}$.

Performance figure of merit

Entanglement of formation (E_F)

Inherently, due to the multi-excitation component in the generated photon–spin-wave state, background noise and dark counts, part of the detector counts will indicate randomly polarized photons. Therefore, we model the experimental imperfections as a depolarizing channel, obtaining in each memory mode a Bell Werner-like state $\rho_{|\psi\rangle}$ given by

$$\rho_{|\psi\rangle} = \frac{(1-V)}{4} \hat{\mathbb{I}} + V|\psi\rangle\langle\psi|, \quad (6)$$

where $|\psi\rangle$ is the selected Bell state $|\psi\rangle \in \{|\Psi_{\pm}\rangle, |\Phi_{\pm}\rangle\}$ and V gives the interference visibility for a Bell-state measurement (BSM). The first term $(1-V)/4 \times \hat{\mathbb{I}}$ corresponds to the introduced white noise.

The entanglement as a resource can be quantified with the entanglement of distillation $E_D(\rho_{|\psi\rangle}^{\otimes n}) = m/n$, which gives the number m of pure states $|\psi\rangle$ that can be distilled from n copies of $\rho_{|\psi\rangle}$ in the limit of $n \rightarrow \infty$. In the opposite scenario the entanglement of formation $E_F(\rho_{|\psi\rangle}^{\otimes n}) = m/n$ gives the required number m of pure states $|\psi\rangle$ required to create n copies of $\rho_{|\psi\rangle}$. As entanglement of distillation is generally difficult to calculate,

we assume an optimistic scenario and use entanglement of formation $E_F(\rho_{|\psi\rangle}) \geq E_D(\rho_{|\psi\rangle})$ for the entangled bits (ebits) content of a single generated $\rho_{|\psi\rangle}$ state. For a Bell Werner-like state $\rho_{|\psi\rangle}(V)$ an exact expression for $E_F(V)$ has been given in Refs. [38, 39]. We note that other entanglement monotones are known [40] to give tighter bounds on E_D yet for simplicity and taking into account the estimative character of our calculations we use E_F .

Ebit rate per unit repeater cost (Q)

The ebit rate R quantifies the amount of distributed entanglement bits per unit time. The average time T_{tot} between successful entanglement distributions over the total distance L , gives the protocol connection rate $1/T_{\text{tot}}$ and the average entanglement of formation $\langle E_F(V) \rangle$ of transmitted states yields the ebit content per connection, thus the ebit rate is given by:

$$R = \langle E_F(V) \rangle / T_{\text{tot}}. \quad (7)$$

With a given total connection distance L , the number of employed repeater nodes N can be optimized to yield the highest ebit rate; however, in design of practical repeater links the infrastructure cost must be taken into consideration as well. To account for such a limitation, we choose the ebit rate per unit repeater node cost as our figure of merit:

$$Q(N, L) = R(N, L) / N, \quad (8)$$

and optimize it over the number of nodes N for each L :

$$N^*(L) = \arg \max_N Q(N, L). \quad (9)$$

Quasi-deterministic entanglement generation

Let us consider an exemplary link with $p_1 = (\chi\eta_m\eta_t)^2$, where η_m denotes the multi-mode single-photon detection efficiency and η_t the transmission loss at $L_0/2$ distance between a memory and the CMS. To keep the multi-excitation probability low, the excitation probability is kept on the order of a few percents. Here, we take $\chi = 0.05$. Multimode detection compatible with thousands of spatial modes can be realized with single-photon cameras e.g. a CMOS camera with an image intensifier [34], novel photon-counting CMOS sensor [41] or arrays of avalanche or superconducting detectors [42], or simply many detectors. The camera-based solutions would be most suitable for free space transmission with 800 nm light, yielding at least 20% detection efficiency. On the other hand, in the telecom band one would have to use quantum frequency conversion techniques (best overall efficiencies of the order of 30% [10]) adapted for many modes along with detector arrays. Overall, we will assume detection efficiency $\eta_m = 0.2$ and consider telecom wavelength transmission over a fibre with attenuation of around $\alpha = 0.2$ dB/km. For WV-MUX we will

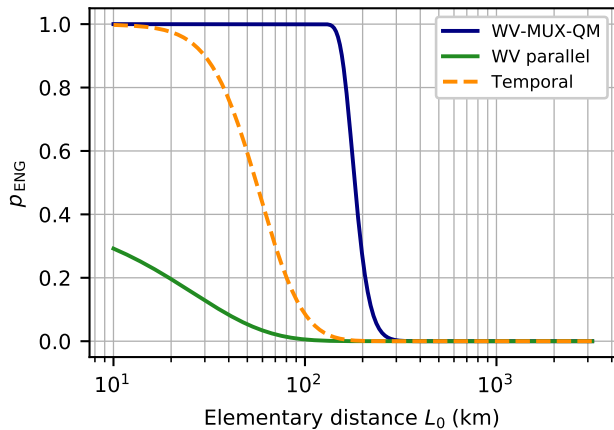


Figure 5. Probability of entanglement generation in an elementary quantum repeater link p_g as a function of the inter-node distance L_0 . Wavevector multiplexed architecture (WV-MUX-QM) is compared with a similar wavevector multimode (WV parallel) system without multiplexing, and with a Temporal multimode platform. See main text for model parameters.

assume $M = 5500$ theoretically attainable in an experimentally demonstrated system as detailed in *Wavevector range* section. Figure 5 depicts the p_g as a function of elementary distance L_0 for WV-MUX-QM-based link, compared to $p_g^{(\text{parallel})}$ for a wavevector multimode system where modes are connected in parallel without multiplexing i.e. i -th mode of A can be connected only with i -th mode of B . Additionally, we consider *temporal* multimode system employing fast single-mode single-photon detection with high detection efficiency $\eta_s \approx 0.9$ and high photon generation efficiency $\chi = 0.47$ across $M = 50$ temporal modes. Noticeably, the entanglement generation is quasi-deterministic for WV-MUX-QM system up to around $L_0 \approx 150$ km.

Mode-specific entanglement quality

Spin-wave decoherence

The multi-photon contribution and noise can be quantified with the second order intensity cross-correlation between the write-out and read-out photons as given by:

$$g^{(2)}(\mathbf{k}_w, \mathbf{k}_r) = \frac{\langle n_w(\mathbf{k}_w)n_r(\mathbf{k}_r) \rangle}{\langle n_w(\mathbf{k}_w) \rangle \langle n_r(\mathbf{k}_r) \rangle}, \quad (10)$$

where $n_w(\mathbf{k}_w)$ ($n_r(\mathbf{k}_r)$) refers to the number of write-out (read-out) photons with wavevector \mathbf{k}_w (\mathbf{k}_r) detected in a single experiment repetition, and the average $\langle \cdot \rangle$ is taken over the repetitions. With low average photon numbers $n \ll 1$ we can approximate $g^{(2)}(\mathbf{k}_w, \mathbf{k}_r) \approx p_{w,r}/(p_w p_r)$, where $p_{w,r} \equiv p_{w,r}(\mathbf{k}_w, \mathbf{k}_r)$ is the total probability of observing a coincidence between write-out and read-out

photons with wavevectors \mathbf{k}_w and \mathbf{k}_r , respectively, and $p_w \equiv p_w(\mathbf{k}_w)$ ($p_r \equiv p_r(\mathbf{k}_r)$) gives the marginal probability of observing a write-out (read-out) photon with wavevector \mathbf{k}_w (\mathbf{k}_r). Coincidences can be divided into uncorrelated events and those originating from the correct memory operation $p_{w,r} = p_w p_r + p_{w,r}^{(\text{signal})}$. Let us select the highest-correlated modes $\mathbf{k}_r = -\mathbf{k}_w = \mathbf{k}$. If we denote the single-photon detection efficiency by η , read-out efficiency by η_r and the probability of a noise photon in the read-out path as B , we get the following probabilities $p_{w,r}^{(\text{signal})} = \eta^2 \eta_r \chi$, $p_w = \eta \chi$, $p_r = \eta \eta_r \chi + B \eta$ which gives [32]:

$$g^{(2)}(\mathbf{k}, -\mathbf{k}) \approx 1 + \left(\chi + \frac{B}{\eta_r} \right)^{-1}. \quad (11)$$

In general, noise and read-out efficiency depend on the memory storage duration, subsequently deteriorating $g^{(2)}$. For clarity, we shall include the B/η_r term into a time-dependent effective $\tilde{\chi}(t) = \chi + B(t)/\eta_r(t)$.

Visibility reduction from uncorrelated coincidences
Among the registered coincidences between the write-out and read-out photons there is a number of noise pairs originating from dark counts, losses and multiphoton excitations. Importantly, in WV-MUX-QM such noise photons attain horizontal or vertical polarization equiprobably, reducing the visibility parameter of the generated state $V(\mathbf{k})$. To derive $V(\mathbf{k})$ explicitly let us consider the second order cross-correlation, as given by Eq. (10). For a maximally correlated pair of write-out $\mathbf{k}_w = \mathbf{k}$ and read-out $\mathbf{k}_r = -\mathbf{k}$ wavevectors and with low average photon numbers $n \ll 1$ we have $g^{(2)}(\mathbf{k}, -\mathbf{k}) \approx p_{w,r}/(p_w p_r)$, where $p_{w,r} \equiv p_{w,r}(\mathbf{k})$ is the single-experiment probability of observing a coincidence between a write-out and read-out photon and $p_w \equiv p_w(\mathbf{k})$ ($p_r \equiv p_r(-\mathbf{k})$) denotes the marginal probability of observing a write-out (read-out) photon. The coincidence probability can be written as $p_{w,r} = g^{(2)} p_w p_r$, with $g^{(2)} \equiv g^{(2)}(\mathbf{k}, -\mathbf{k})$. The state visibility can be measured in a Bell state measurement (BSM) configuration. Consider coincidence counts between write-out and read-out photons with a polarization BSM. We can denote $V(\mathbf{k}) = (p_{w,r}^{(+)} - p_{w,r}^{(-)}) / (p_{w,r}^{(+)} + p_{w,r}^{(-)})$, where superscripts (\pm) denote measurements settings with maximally constructive (+) or destructive (-) interference. In (-) settings only noise coincidences are registered i.e. $p_{w,r}^{(-)} = p_w p_r$ while $p_{w,r}^{(+)} = p_{w,r} = g^{(2)} p_w p_r$. Therefore, the visibility can be written as

$$V(\mathbf{k}) = \frac{g^{(2)}(\mathbf{k}, -\mathbf{k}) - 1}{g^{(2)}(\mathbf{k}, -\mathbf{k}) + 1}. \quad (12)$$

We note that a \mathbf{k} mode has a finite extent in \mathbf{k} -space and for an efficient implementation of a BSM, it is necessary to integrate the coincidences over the mode extent, effectively averaging the visibility, given by Eq. (12), in \mathbf{k} -space.

Memory decoherence

The memory lifetime τ , limited by the spin-wave decoherence rate, sets a relationship between the ebit content of the generated state E_F and the storage time t . For an atomic ensemble cooled in a magneto-optical trap (MOT) and stored in a dipole trap, the main spin-wave decoherence mechanism is through the thermal motion of individual atoms [21, 32] which distorts the spatial structure of a spin-wave. Intuitively, an atom travelling out of its initial position has the more detrimental effect on the spin-wave, the finer spatial details of the spin-wave are. Therefore, we expect τ to be mode-specific and grow with lower spin-wave wavevector modulus $K \equiv |\mathbf{K}|$. The exact result follows from a thermal evolution of a spin-wave state and is given by the overlap of the evolved and the initial spin-wave states $|\langle S_{\mathbf{K}}(0)|S_{\mathbf{K}}(t)\rangle|^2 \propto \exp(-t^2/\tau(K)^2)$ which has a Gaussian form and where $\tau(K) = \gamma/K$ with the proportionality constant $\gamma = \sqrt{m/k_B T}$ depending on the atomic mass of Rb-87 m , ensemble temperature T and Boltzmann constant k_B . For typically attainable temperatures $T \approx 1 \mu\text{K}$, $\gamma \approx 10^5 \mu\text{s}/\text{mm}$.

Effectively, the spin-wave decoherence decreases the readout efficiency $\eta_r(t) = \exp(-t^2/\tau(K)^2)$. We shall further assume a constant noise level $B(t) = \text{const}$. This way, we can account for the visibility deterioration by considering the cross-correlation $g^{(2)}(\mathbf{k}, -\mathbf{k}; t) \approx 1 + \exp(-t^2/\tau(K)^2)/\tilde{\chi}(0)$ and using Eq. (12) to arrive at the time-dependent average visibility:

$$V(K, t) = \frac{1}{1 + 2\tilde{\chi}(0) \exp(t^2/\tau(K)^2)}, \quad (13)$$

where we shall approximate $\tilde{\chi}(0) \approx \chi$ for experimentally feasible conditions.

Wavevector range

Let us consider modes from $K_{\min} = 10 \text{ mm}^{-1}$ to $K_{\max} = 10^3 \text{ mm}^{-1}$ which constitute a practically feasible range of captured emission angles $2 \times 0.073^\circ$ to $2 \times 7.3^\circ$ while still allowing to route the write and read beams. In such a case we get $\tau(K_{\min}) = 10 \text{ ms}$ and $\tau(K_{\max}) = 100 \mu\text{s}$. Importantly, the number of modes in a range $[K, K + dK]$ is $2\pi K \beta dK$ which grows with K , and where β is the K -space mode density. In our previous work [21] we have determined the number of modes in a WV-MUX-QM by performing a singular value decomposition on experimentally collected data. The obtained mode density $\beta = 3.5 \times 10^{-3} 1/\text{mm}^2$ with our choice of K_{\min} and K_{\max} corresponds to the total number of $M = 5500$ modes, where implicitly we have halved the number of modes to enable the generation of polarization entangled states in M pairs of wavevector modes, required for a two-photon quantum repeater protocol.

The range of K modes is limited by the geometry of the optical setup and the size and resolution of the im-

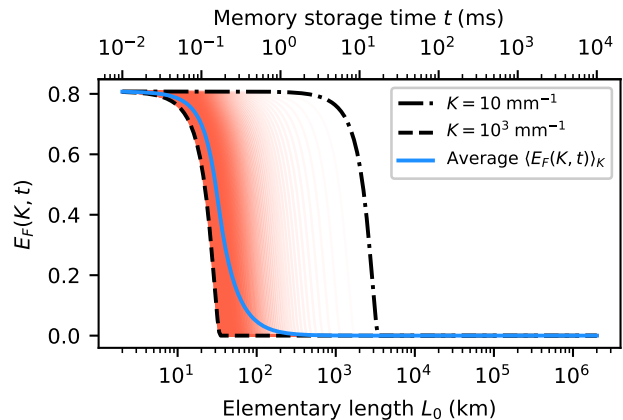


Figure 6. Entanglement of formation $E_F(K, L_0/c)$ as a measure of ebit content in entangled states of a photon and a spin-wave with wavevector modulus K , stored for a memory time L_0/c required in entanglement generation over an inter-node elementary distance L_0 . Red curves correspond to specific memory modes while the blue curve gives the average over the modes. The black dashed and dot-dashed curves indicate the $E_F(K_{\max}, t)$ and $E_F(K_{\min}, t)$, respectively, with $K_{\max} = 10^3 \text{ mm}^{-1}$, $K_{\min} = 10 \text{ mm}^{-1}$ corresponding to the modes with the highest and lowest spin-wave wavevector.

age sensor in a single-photon sensitive camera [34]. The atomic ensembles is assumed to be cooled in a magneto-optical trap and further trapped in a dipole trap, reaching the temperature of a $1 \mu\text{K}$ which gives $\gamma \approx 10^5 \mu\text{s}/\text{mm}^{-1}$ amounting to a relatively short lifetime of around $100 \mu\text{s}$ for K_{\max} mode. Clearly, there is little point in observing quickly decaying modes for $K > K_{\max}$. The operation of the memory requires counter-propagating write and read beams [21], limiting the observable emission at small angles. With 800 nm wavelength, $K_{\min} = 10 \text{ mm}^{-1}$ amounts to ca. $200 \mu\text{m}$ diameter in the far-field left for write/read beam routing, assuming a lens of focal lengths $f = 100 \text{ mm}$. Such a configuration gives the diameter of the total observed far-field of around 1 inch which is compatible with standard optical elements and feasible to be imaged onto a commercially available $10 \times 10 \text{ mm}$ CMOS sensors with around $1 \text{ px} = 10 \mu\text{m}$ pixel size. With a properly adjusted magnification the characteristic Gaussian mode size 2σ of around $2 \times 4.8 \text{ mm}^{-1}$ corresponds to around 2.5 px on the camera sensor [21].

Mode performance

The ebit content of states generated across different K modes varies, as illustrated in Fig. 6. As the number of modes with a given K grow with K , most of the modes occupy quickly decaying high- K modes, reducing the average entanglement of formation $\langle E_F(K, t) \rangle_K$.

Quantum repeaters architecture

Hierarchy

Hierarchical protocols like DLCZ or two-photon protocols divide the N nodes pair-wise recursively to form a binary tree. There is a conceptual advantage in a such an approach as one only needs to consider the connection time between two sub-nets at each nesting level; however, if one sub-net fails and needs to start from the entanglement generation at the lowest level, there is a tremendous waiting time overhead for classical communication to synchronize the manoeuvre. The average requirement for memory storage time may many times exceeds the direct communication time L/c between the parties.

On the other hand, in ahierarchical architecture all nodes would operate synchronized only by a classical clock with period L_0/c and without any feedback. While the requirements for memory storage time are substantially lower, all nodes must succeed simultaneously for an overall success. With limited efficiencies of memories and detectors, successful generation becomes exponentially difficult with the increasing number of nodes.

Semihierarchical architecture has been proposed [25] as an intermediate regime. Nodes communicate with a central station located mid-way between the final parties, which waits until all nodes successfully generate the entanglement and synchronizes entanglement connection. While the ENC has to succeed simultaneously across all nodes, the nodes which succeed with ENG wait for other nodes. Such an approach improves the probability of success per protocol repetition as compared with ahierarchical approach and has lower memory time requirements than hierarchical architecture.

Regardless of the architecture, the average time for successful entanglement distribution can be modularly written as

$$T_{\text{tot}} = T_r / (P_{\text{ENG}} P_{\text{ENC}} \eta_s^2 \eta_x^2), \quad (14)$$

where T_r is the (average) repetition period of the protocol, P_{ENG} the probability of a successful entanglement generation between all pairs of ensembles, P_{ENC} the probability of a successful entanglement connection across all nodes and $\eta_s^2 \eta_x^2$ the probability of detecting the entangled photons at final parties with η_s being the efficiency of single-photon detectors and η_x of multiplexing.

Ahierarchical architecture

Let us assume that the main delay in the protocol is the transmission time of a write-out photon between a node and a CMS and of the which-mode information back to the node i.e. $T_r = L_0/c$, where we take $c = 0.2$ km/ μ s for a fibre transmission. For the protocol to succeed with $N = L/L_0 + 1$ nodes, we need to generate entanglement (ENG) between $N - 1$ memories and perform

first-stage ENC (further ENC) between $\approx \lceil (N - 2)/2 \rceil$ (between $\lfloor (N - 2)/2 \rfloor$) memories. Additionally multiplexing (MUX) is required before each ENC and fist-stage ENC (fENC). Let us denote the efficiencies of ENG in a single mode, fENC, ENC and MUX by p_g , p_f , p_e , η_x , respectively. In the ahierarchical architecture all nodes blindly assume that all other nodes succeeded with ENG and proceed with the ENC. The overall probability for ENG is given by

$$P_{\text{ENG}} = p_g^{N-1}, \quad (15)$$

with p_g given by Eq. (5), while for ENC it is

$$P_{\text{ENC}} = p_f^{\lceil (N-2)/2 \rceil} p_e^{\lfloor (N-2)/2 \rfloor} \eta_x^N. \quad (16)$$

In standard two-photon protocols p_e is upper bounded by $1/2$ and $p_f = p_e/4$ due to post-selecting on coincidence patterns chosen to project the state of connected memories onto a Bell state [8].

Semihierarchical architecture

For the rates in semihierarchical architecture we follow the derivations by Liu *et al.* [25] with a slight modification to match the two-photon protocol and the WV-MUX-QM platform. Let us start with Eq. (14). We shall modify the T_r/P_{ENG} factor to be now an expectation value over the distribution of waiting times for all nodes to accomplish entanglement generation. Importantly, there is an additional waiting overhead L/c for two-way communication with the central station. The factor T_r/P_{ENG} now reads $T_r/P_{\text{ENG}} = (L_0/c \times f(N, p_g)/p_g + L/c)$ where $f(N, p_g)$ gives the expected number of ENG repetitions to accomplish ENG between N nodes with p_g given by Eq. (5) or Eq. (4) for multiplexed and parallel platforms, respectively. The factor $f(N, p_g)$ is given by:

$$f(N, p_g) = p_g \sum_{j=1}^{\infty} j \times \{ [1 - (1 - p_g)^j]^N - [1 - (1 - p_g)^{j-1}]^N \}. \quad (17)$$

Limitations

Maximal range

A non-zero ebit content $E_F(V(t_m)) > 0$ of the generated state after storage time t_m requires visibility $V(t_m)$ above $1/3$ which is equivalent to $\chi \exp[t_m^2/\tau(K)^2] < 1$ by Eq. (13).

In the case of ahierarchical architecture the storage time is always $t_m = L_0/c$ giving $L_0^{(\text{max})} = c\tau(K)\sqrt{\log(1/\chi)}$ and so $L_{\text{max}} = NL_0^{(\text{max})}$. For $\chi = 0.05$ and $c = 0.2$ km/ μ s we have for the longest-live $K = 10$ mm $^{-1}$ mode $\tau(K) = 10$ ms and $L_0^{(\text{max})} \approx 3.5 \times 10^3$ km.

Let us require that 1% of all modes have a non-zero ebit content, this corresponds to a range of K from 10 mm^{-1} to 100 mm^{-1} with the lowest $\tau(K = 100 \text{ mm}^{-1}) = 1 \text{ ms}$ and in this case $L_0^{(\max)} \approx 350 \text{ km}$. This characteristic range is clearly visible in Fig. 6.

For the semihierarchical architecture and assuming all nodes succeed with entanglement generation in the first try, the total storage time for each memory is $t_m = (L + L_0)/c$. Employing Eq. (13), the requirement on the memory coherence time becomes:

$$\tau(K) > 2 \frac{L + L_0}{c \log(1/\chi)}, \quad (18)$$

which for a fixed $\tau(K)$ sets the maximal range

$$L_{\max} = \frac{N - 1}{N} \frac{\tau(K)}{2} c \log\left(\frac{1}{\chi}\right), \quad (19)$$

where $L + L_0 = LN/(N - 1)$. For $\chi = 0.05$, $\tau(K) = 10 \text{ ms}$, $c = 0.2 \text{ km}/\mu\text{s}$, the maximal distance is ca. $L_{\max} \approx 3 \times 10^3 \text{ km}$ for large $N \gg 1$.

Entanglement connection probability

The tremendous number of modes in WV-MUX-QM platform combined with flexible multiplexing offers a quasi-deterministic entanglement generation for extended distances between the elementary nodes. As depicted in Fig. 7a, the probability of a successful ENG between any of M^2 combinations of modes remains nearly 100% even with significant optical losses (1% transmission over 100 km). Importantly, lifetime of spin-waves occupying different K modes quickly deteriorates with increasing K , making only a small fraction of modes feasible for ENG over large L_0 , as indicated by the average entanglement of formation $\langle E_F(K, L_0/c) \rangle_K$ which is depicted in Fig. 7a. This in turn limits the maximal L_0 which settles at the level of around 150 km, as illustrated in Fig. 7c. With increasing L and limited L_0 the optimal number of nodes N^* quickly increases, which is clearly visible in Fig. 7b. Conversely, as indicated by Eq. (14), the probability of a simultaneous success of ENC across all nodes, scaling with the power of N^* , rapidly decreases.

A possible solution would be to entangle many pairs of modes during ENG and perform a multiplexed ENC amending the deteriorating scaling with the power of N^* .

Telecom wavelength and multimode transmission

While we start our discussion from an experimental realization of a WV-MUX-QM platform [21] which employs a $\approx 800 \text{ nm}$ light-matter interface, there have been several demonstrations of Rb-87 atomic memories working in the telecom regime thanks to external or

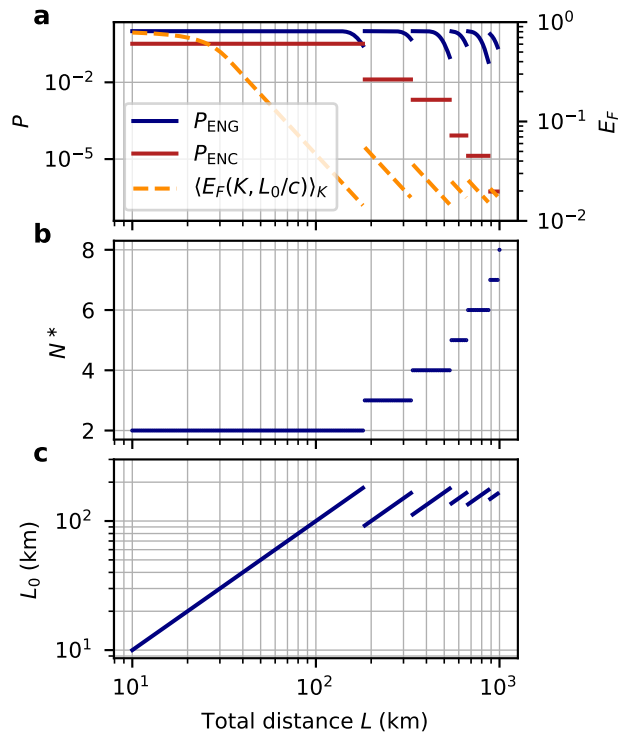


Figure 7. Performance measures for WV-MUX-QM platform in ahierarchical architecture with a total distance L . **a** Total probability of entanglement generation in all nodes simultaneously P_{ENG} is nearly constant and close to unity while total probability of entanglement connection between all nodes and final detection of entangled photons P_{ENC} falls significantly as the optimal total number of nodes N^* – depicted in **b** – grows. **c** Elementary distance between adjacent nodes L_0 for the optimal number of nodes N^* .

in-memory conversion [15, 43–45]; therefore, an experimental realization could build on these results and exploit wavevector multiplexing together with a telecom light-matter interface.

Another technically challenging task would be to implement multimode transmission channel. One way would be to use free-space which is inherently multimode, yet sensitive to atmospheric conditions and requiring expensive optical infrastructure. Another solution are multimode fiber transmission systems e.g. consisting of an array of single-mode telecom fibers. Importantly, commercially available fiber coupled microlens arrays [46] enable efficient coupling of particular memory modes to the transmission channel and make the solution practically feasible.

Rate comparison

We have compared the performance of several physical platforms as candidates for a quantum repeater nodes in

ahierarchical and semihierarchical architecture. For each total distance between the parties L we select a number of nodes $N \geq 2$ which maximizes the entanglement transfer rate per node number given by Eq. (8): $N^*(L) = \arg \max_N \langle Q(N, L) \rangle_{K,t}$ with the average $\langle \cdot \rangle$ taken over the distribution of required memory times t across realizations and the performance of individual K -modes in a single realization. The comparison encompasses the wavevector multiplexed quantum memory (*WV-MUX-QM*), parallel operation (*parallel*, without multiplexing) of a wavevector multimode quantum memory, temporal multimode quantum memory (*temporal*) and a state-of-the-art single-mode, long-lifetime atomic quantum memory in an optical lattice (*lattice*). For reference we consider a direct entanglement generation via a single spontaneous parametric down conversion (SPDC) source located midway between the parties.

Figure 8 depicts the average time for a successful transfer and detection of a single ebit $T = 1/(N^* \times Q(N^*, L))$ for the compared platforms, along typical time scales. Above ca. 300 km *WV-MUX-QM* in the ahierarchical architecture outperforms a direct SPDC source. For ca. 550 km the average time for the *WV-MUX-QM* platform is ca. 6 minutes while for an SPDC source it amounts to over 2 days; for ca. 700 km the average times are around 40 minutes versus over 5 years.

Importantly, the assumed parameters correspond to the state-of-the-art experimentally attainable systems; therefore, while the current ebit rates remain impractical for most technological applications, wavevector multiplexing appears to be a promising technique for near-term quantum repeaters.

As illustrated in Fig. 9, the optimal number of nodes $N^*(L)$ grows relatively slowly with L for the *WV-MUX-QM* platform, reflecting the ability to quasi-deterministically generate entanglement over extended inter-node elementary distances L_0 .

One of the limiting factors for the *WV-MUX-QM* architecture is the mode-dependent memory lifetime which quickly degrades the ebit content of a significant number of modes. For example, for an elementary distance of $L_0 = 150$ km, the state generation is still quasi-deterministic, while the entanglement of formation yields on average $\langle E_F(K, t = L_0/c) \rangle_K \approx 2 \times 10^{-2}$. Importantly, despite very low ebit content per state, the probabilistic protocols which enable single-copy distillation of a pure Bell state [47].

III. DISCUSSION

In this work we show the feasibility of wavevector multiplexed quantum memories (*WV-MUX-QM*) for near-term quantum repeaters, as an alternative to temporally, spectrally or spatially-multimode platforms. Remaining within the constraints of current technology, we consider an extension of an experimentally demonstrated *WV-MUX-QM* platform [21] combined with available meth-

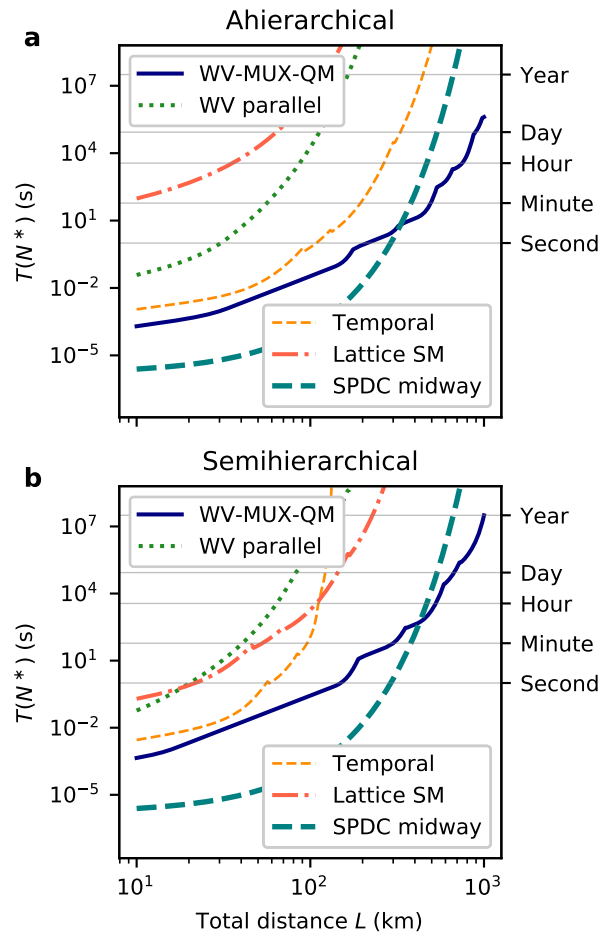


Figure 8. Average time T for a successful transfer of an ebit between parties separated by distance L , employing either a central SPDC source as a generator of polarization-entangled pairs of photons (*SPDC*) or a quantum repeater architecture (*WV-MUX-QM*, *WV parallel*, *Temporal*, *Lattice SM*), either **a** - ahierarchical or **b** - semihierarchical. Experimentally feasible physical realizations of a repeater node are compared. The number of repeater nodes N is optimized for a maximal ebit rate per number of nodes Q .

ods of optical multiplexing and fast spatially-resolved single-photon detection. We harness the tremendous number of modes $M \approx 5500$ theoretically available in *WV-MUX-QM* to design a robust scheme for polarization entanglement generation (ENG) between distant quantum repeater nodes. Importantly, the designed ENG scheme allows to connect any pair of modes giving M^2 possibilities and providing a quasi-deterministic ENG at ca. 150 km of telecom fibre.

We extend the *WV-MUX-QM* setup with a specifically designed Mach-Zehnder interferometer allowing implementation of a two-photon interference-based quantum repeater protocol [8] robust to optical phase fluctuations which deteriorate the performance of the standard DLCZ protocol. Additionally, we consider each

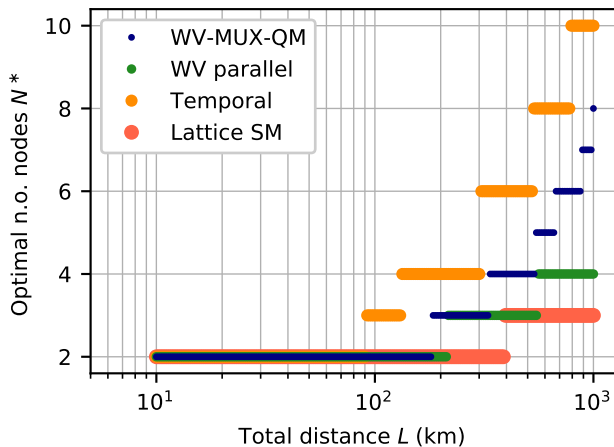


Figure 9. Optimal number of repeater nodes N^* maximizing the ebit rate per number of nodes Q for a given total distance L . Physical platforms for the repeater node are compared within the ahierarchical architecture.

memory mode separately by employing a mode-specific decoherence model and calculate the ebit transfer rate by modelling the losses and noise as an depolarizing channel. For the resource-efficient comparison of different quantum repeater platforms, we establish an ebit transfer rate between the final parties per number of employed quantum repeater nodes as our figure of merit.

Finally, we analyse WV-MUX-QM in recently proposed semihierarchical quantum repeater architecture as well as a simple ahierarchical architecture and find the main limitations of the WV-MUX-QM platform. Importantly, while the entanglement generation can be quasi-deterministic for over a hundred km inter-node distance L_0 , most of the memory modes have a short lifetime deteriorating the ebit content of the generated states with an increasing L_0 . Conversely, the total distance L is mainly limited by the growing number of nodes N with a limited inter-node distance $L_0 \lesssim 150$ km. Importantly, while multiplexing remedies the fundamental transmission losses inherent to the ENG stage, the entanglement connection (ENC) remains single-mode. Since ENC results are post-selected, even with ideal detectors and memory retrieval efficiency, the probability of a successful ENC is severely limited. With the growing number of nodes N , the requirement for a simultaneous success of all $N - 1$ ENCs constitutes the main factor limiting the total distance L . Furthermore, we envisage that our methods can be also applied to a spatially-multiplexed quantum memory [20], where multiplexing is provided by addressing different micro-ensembled at different times with AODs. Since the WV-MUX-QM platform is capable of flexible processing on the stored spin-waves [22–24], we envisage that, as a remedy to the low total ENC probability, a method could be design to entangle many mode pairs simultaneously during ENG and perform a multiplexed or parallelized ENC, such an

approach is however beyond the scope of this work and may be an interesting avenue for future development.

AUTHOR CONTRIBUTIONS

M.L., M.M. and M.P. jointly conceived the scheme. M.L. developed the theory, performed calculations and wrote the paper with contributions from other authors. M.P. supervised the project.

COMPETING INTERESTS

The authors declare that there are no competing interests.

DATA AVAILABILITY

Data generated during the study is available from the corresponding author upon reasonable request.

ACKNOWLEDGMENTS

This work was funded by Ministry of Science and Higher Education (Poland) grants No. DI2016 014846, DI2018 010848; National Science Centre (Poland) grants No. 2016/21/B/ST2/02559, 2017/25/N/ST2/01163, 2017/25/N/ST2/00713; Foundation for Polish Science MAB 4/2017 “Quantum Optical Technologies”.

The “Quantum Optical Technologies” project is carried out within the International Research Agendas programme of the Foundation for Polish Science co-financed by the European Union under the European Regional Development Fund. M.P. was supported by the Foundation for Polish Science START scholarship.

We would like to thank W. Wasilewski for fruitful discussions and K. Banaszek for the generous support.

METHODS

In our comparison we assume that the transmitted ebit has to be detected at final parties to be useful i.e. we include the efficiency of detectors at the first and the last node. The optical transmission is assumed to be carried via telecom fibres characterized by attenuation of $\alpha = 0.2$ dB/km which gives the transmission efficiency over length z of $\eta_t(z) = 10^{-\alpha z/10}$. The success probability for a single ENG is taken as $p_1 = (\chi\eta_t(L_0/2)\eta_m)^2$, while for ENC to be $p_e = (\eta_r\eta_s)^2/2$. Whenever we are detecting single-photons in a single spatial mode, we assume the detector efficiency of $\eta_s = 0.9$ [48] and for the multimode detection $\eta_m = 0.2$ [34], both corresponding to experimentally attainable values. Model parameters are summarized in Tab. I.

Model parameters

Platform	M	χ	τ (ms)	η_x	η_r	η_s	η_m
WV-MUX-QM	5500	0.05	$(10^2 \text{ mm}^{-1})/K$	0.9	0.7	0.9	0.2
WV parallel	5500	0.05	$(10^2 \text{ mm}^{-1})/K$	1	0.7	0.2	0.2
Temporal	50	0.47	1	1	0.71	0.9	0.9
Lattice SM	1	0.05	220	1	0.76	0.9	0.9

Table I. Summary of model parameters for the comparison of quantum repeater platforms. Wavevector-multiplexed (WV-MUX-QM) and wavevector parallel (WV parallel) atomic quantum memories are compared with solid-state temporal multimode and single-mode state-of-the-art atomic memory. Parameters are estimated from current state-of-the-art experimental demonstrations.

For the SPDC midway source we assume a repetition rate of $f_{\text{rep}} = 80$ MHz, the probability of generating a pair of correlated photons $\chi = 0.01$ and perfect visibility $V = 1$ giving $E_F = 1$ i.e. one ebit per successful connection. The average time for an ebit transmission is therefore $T_{\text{SPDC}}(L) = \chi(\eta_t(L)\eta_s)^2 f_{\text{rep}}$.

For the *WV-MUX-QM* and *WV parallel* models we assume an atomic Rb-87 quantum memory with wavevector modes. The probability of generating a pair of a photon and a spin-wave is assumed to be $\chi = 0.05$ which is found close to the optimal for long total distances $L \geq 100$ km. The readout efficiency is assumed at the state-of-the-art experimentally-demonstrated level of around 70% [49] i.e. $\eta_r = 0.7$.

For *WV-MUX-QM* the multiplexing efficiency is taken to be $\eta_x = 0.9$ which is a realistic estimate with an optical switch based on acousto-optical deflectors, such as demonstrated in ref. [50] and detailed in *Multiplexing* section. The probability of entanglement generation between two nodes is in this case given by Eq. (5).

For *WV parallel* operation there is no loss at multiplexing thus $\eta_x = 1$, and the probability of entanglement, given by Eq. 4, scales with M and not M^2 . Additionally, lack of multiplexing requires a mode-resolved BSM for ENC stage, reducing the detection efficiency at this stage from $\eta_s = 0.9$ to $\eta_m = 0.2$.

For *Temporal* multiplexing we consider solid-state quantum memories with separate single-photon sources (SPS) e.g. quantum dot sources and memories exploiting atomic frequency comb in rare-earth-ion-doped solids. While multiple degrees of freedom (DoF) multiplexing has been demonstrated in such systems [51], there is no straight-forward way to harness additional DoF to implement two-photon protocols without the overhead of multiple pairs of SPS and QM at each node. Therefore, we assume temporal modes are processed independently and Eq. (4) applies. The assumed number of modes is as reported in the state-of-the-art experimental demonstrations $M = 50$ with a lifetime of 1 ms for all modes [52]. For the assumed quantum dot SPS a 66% generation efficiency has been demonstrated [53]. The total memory storage and retrieval efficiency is taken to be 50%, which is around the state-of-the-art results [54], and assumed to be equally distributed over the storage $\chi = 0.66/\sqrt{2} \approx 0.47$ and the retrieval $\eta_r = 1/\sqrt{2} \approx 0.71$ efficiencies.

We note that across various implementations of solid state quantum memories in doped crystals, there is a high discrepancy between storage times, efficiency, number of modes and multiplexing capabilities. Instead of considering a single crystal or protocol, for the purpose of this comparison, we optimistically assume a platform performing reasonably close to all of the state-of-the-art parameters.

Finally, the *Lattice SM* platform refers to a single mode (SM) atomic memory with atoms trapped in an optical lattice which greatly extends the memory lifetime to ca. 220 ms as reported by Yang *et al.* [55]. Simultaneous use of an optical cavity in this experiment increased the readout efficiency to ca. 76%, we thus assume $\eta_r = 0.76$. Other parameters are taken as in the *parallel* case, except the number of modes $M = 1$.

Importantly, for *Lattice SM* and *temporal* platforms, the decoherence is exponential $\exp(-t/\tau)$, while for wavevector multimode memories it has a Gaussian profile $\exp(-t^2/\tau^2)$.

-
- [1] N. Sangouard, C. Simon, H. De Riedmatten, and N. Gisin, *Rev. Mod. Phys.* **83**, 33 (2011).
- [2] S. Wehner, D. Elkouss, and R. Hanson, *Science* **362**, eaam9288 (2018).
- [3] S. Pirandola, C. Ottaviani, G. Spedalieri, C. Weedbrook, S. L. Braunstein, S. Lloyd, T. Gehring, C. S. Jacobsen, and U. L. Andersen, *Nat. Photonics* **9**, 397 (2015).
- [4] S. Pirandola, U. L. Andersen, L. Banchi, M. Berta, D. Bunandar, R. Colbeck, D. Englund, T. Gehring, C. Lupo, C. Ottaviani, J. Pereira, M. Razavi, J. S. Shaari, M. Tomamichel, V. C. Usenko, G. Vallone, P. Villoresi, and P. Wallden, “*Advances in Quantum Cryptography*,” arXiv:1906.01645 (2019).
- [5] W. Zhang, D.-S. Ding, Y.-B. Sheng, L. Zhou, B.-S. Shi, and G.-C. Guo, *Phys. Rev. Lett.* **118**, 220501 (2017).
- [6] H.-J. Briegel, W. Dür, J. I. Cirac, and P. Zoller, *Phys. Rev. Lett.* **81**, 5932 (1998).
- [7] Z. S. Yuan, Y. A. Chen, B. Zhao, S. Chen, J. Schmiedmayer, and J. W. Pan, *Nature* **454**, 1098 (2008).
- [8] B. Zhao, Z.-B. Chen, Y.-A. Chen, J. Schmiedmayer, and J.-W. Pan, *Phys. Rev. Lett.* **98**, 240502 (2007).
- [9] N. Gisin, *Frontiers of Physics* **10**, 100307 (2015).
- [10] Y. Yu, F. Ma, X.-Y. Luo, B. Jing, P.-F. Sun, R.-Z. Fang, C.-W. Yang, H. Liu, M.-Y. Zheng, X.-P. Xie, W.-J. Zhang, L.-X. You, Z. Wang, T.-Y. Chen, Q. Zhang, X.-H. Bao, and J.-W. Pan, *Nature* **578**, 240 (2020).
- [11] O. A. Collins, S. D. Jenkins, A. Kuzmich, and T. A. B. Kennedy, *Phys. Rev. Lett.* **98**, 060502 (2007).

- [12] S. B. Dam, P. C. Humphreys, F. Rozpedek, S. Wehner, and R. Hanson, *Quantum Sci. Technol.* **2**, 034002 (2017).
- [13] C. Simon, H. de Riedmatten, M. Afzelius, N. Sangouard, H. Zbinden, and N. Gisin, *Phys. Rev. Lett.* **98**, 190503 (2007).
- [14] C. Simon, H. De Riedmatten, and M. Afzelius, *Phys. Rev. A* **82**, 010304 (2010).
- [15] W. Chang, C. Li, Y.-K. Wu, N. Jiang, S. Zhang, Y.-F. Pu, X.-Y. Chang, and L.-M. Duan, *Phys. Rev. X* **9**, 041033 (2019).
- [16] N. Sinclair, E. Saglamyurek, H. Mallahzadeh, J. A. Slater, M. George, R. Ricken, M. P. Hedges, D. Oblak, C. Simon, W. Sohler, and W. Tittel, *Phys. Rev. Lett.* **113**, 053603 (2014).
- [17] Y. Wen, P. Zhou, Z. Xu, L. Yuan, H. Zhang, S. Wang, L. Tian, S. Li, and H. Wang, *Phys. Rev. A* **100**, 012342 (2019).
- [18] L. Tian, Z. Xu, L. Chen, W. Ge, H. Yuan, Y. Wen, S. Wang, S. Li, and H. Wang, *Phys. Rev. Lett.* **119**, 130505 (2017).
- [19] C. Li, N. Jiang, Y.-K. Wu, W. Chang, Y.-F. Pu, S. Zhang, and L.-M. Duan, *Phys. Rev. Lett.* **124**, 240504 (2020).
- [20] Y.-F. Pu, N. Jiang, W. Chang, H.-X. Yang, C. Li, and L.-M. Duan, *Nat. Commun.* **8**, 15359 (2017).
- [21] M. Parniak, M. Dąbrowski, M. Mazelanik, A. Leszczyński, M. Lipka, and W. Wasilewski, *Nat. Commun.* **8**, 2140 (2017).
- [22] M. Parniak, M. Mazelanik, A. Leszczyński, M. Lipka, M. Dąbrowski, and W. Wasilewski, *Phys. Rev. Lett.* **122**, 063604 (2019).
- [23] M. Mazelanik, M. Parniak, A. Leszczyński, M. Lipka, and W. Wasilewski, *npj Quantum Inf.* **5**, 22 (2019).
- [24] M. Lipka, A. Leszczyński, M. Mazelanik, M. Parniak, and W. Wasilewski, *Phys. Rev. Appl.* **11**, 034049 (2019).
- [25] X. Liu, Z.-Q. Zhou, Y.-L. Hua, C.-F. Li, and G.-C. Guo, *Phys. Rev. A* **95**, 012319 (2017).
- [26] D. J. Richardson, J. M. Fini, and L. E. Nelson, *Nat. Photonics* **7**, 354 (2013).
- [27] Y. Ding, D. Bacco, K. Dalgaard, X. Cai, X. Zhou, K. Rottwitt, and L. K. Oxenlowe, *npj Quantum Inf.* **3**, 25 (2017).
- [28] S. K. Liao, H. L. Yong, C. Liu, G. L. Shentu, D. D. Li, J. Lin, H. Dai, S. Q. Zhao, B. Li, J. Y. Guan, W. Chen, Y. H. Gong, Y. Li, Z. H. Lin, G. S. Pan, J. S. Pelc, M. M. Fejer, W. Z. Zhang, W. Y. Liu, J. Yin, J. G. Ren, X. B. Wang, Q. Zhang, C. Z. Peng, and J. W. Pan, *Nat. Photonics* **11**, 509 (2017).
- [29] L. M. Duan, M. D. Lukin, J. I. Cirac, and P. Zoller, *Nature* **414**, 413 (2001).
- [30] Z.-B. Chen, B. Zhao, Y.-A. Chen, J. Schmiedmayer, and J.-W. Pan, *Phys. Rev. A* **76**, 022329 (2007).
- [31] R. Grimm, M. Weidemüller, and Y. B. Ovchinnikov, *Adv. At. Mol. Opt. Phys.* **42**, 95 (2000).
- [32] B. Zhao, Y. A. Chen, X. H. Bao, T. Strassel, C. S. Chuu, X. M. Jin, J. Schmiedmayer, Z. S. Yuan, S. Chen, and J. W. Pan, *Nat. Phys.* **5**, 95 (2009).
- [33] P. Boffi, S. Pietralunga, and M. Martinelli, *Opt. Commun.* **123**, 473 (1996).
- [34] M. Lipka, M. Parniak, and W. Wasilewski, *Appl. Phys. Lett.* **112**, 211105 (2018).
- [35] L. Jiang, J. M. Taylor, and M. D. Lukin, *Phys. Rev. A* **76**, 012301 (2007).
- [36] M. Mazelanik, M. Dąbrowski, and W. Wasilewski, *Opt. Express* **24**, 21995 (2016).
- [37] G. Andersen, P. Gelsinger-Austin, R. Gaddipati, P. Gaddipati, and F. Ghebremichael, *Opt. Express* **22**, 9432 (2014).
- [38] W. K. Wootters, *Phys. Rev. Lett.* **80**, 2245 (1998).
- [39] S. Díaz-Solórzano and E. Castro, “Exact analytical solution of Entanglement of Formation and Quantum Discord for Werner state and Generalized Werner-Like states,” arXiv:1802.05877 (2018).
- [40] E. M. Rains, *IEEE Transactions on Information Theory* **47**, 2921 (2001).
- [41] J. Ma, S. Masoodian, D. A. Starkey, and E. R. Fossum, *Optica* **4**, 1474 (2017).
- [42] E. E. Wollman, V. B. Verma, A. E. Lita, W. H. Farr, M. D. Shaw, R. P. Mirin, and S. Woo Nam, *Opt. Express* **27**, 35279 (2019).
- [43] B. Albrecht, P. Farrera, X. Fernandez-Gonzalvo, M. Cristiani, and H. de Riedmatten, *Nat. Commun.* **5**, 3376 (2014).
- [44] T. Chaneliere, D. N. Matsukevich, S. D. Jenkins, T. A. B. Kennedy, M. S. Chapman, and A. Kuzmich, *Phys. Rev. Lett.* **96**, 093604 (2006).
- [45] A. G. Radnaev, Y. O. Dudin, R. Zhao, H. H. Jen, S. D. Jenkins, A. Kuzmich, and T. A. Kennedy, *Nat. Phys.* **6**, 894 (2010).
- [46] SQS Vláknová optika a.s., “Fiber Coupled Microlens Array,” .
- [47] Z.-W. Wang, X.-F. Zhou, Y.-F. Huang, Y.-S. Zhang, X.-F. Ren, and G.-C. Guo, *Phys. Rev. Lett.* **96**, 220505 (2006).
- [48] F. Marsili, V. B. Verma, J. A. Stern, S. Harrington, A. E. Lita, T. Gerrits, I. Vayshenker, B. Baek, M. D. Shaw, R. P. Mirin, and S. W. Nam, *Nat. Photonics* **7**, 210 (2013).
- [49] Y.-W. Cho, G. T. Campbell, J. L. Everett, J. Bernu, D. B. Higginbottom, M. T. Cao, J. Geng, N. P. Robins, P. K. Lam, and B. C. Buchler, *Optica* **3**, 100 (2016).
- [50] N. Jiang, Y. F. Pu, W. Chang, C. Li, S. Zhang, and L. M. Duan, *npj Quantum Inf.* **5**, 28 (2019).
- [51] T.-S. Yang, Z.-Q. Zhou, Y.-L. Hua, X. Liu, Z.-F. Li, P.-Y. Li, Y. Ma, C. Liu, P.-J. Liang, X. Li, Y.-X. Xiao, J. Hu, C.-F. Li, and G.-C. Guo, *Nat. Commun.* **9**, 3407 (2018).
- [52] P. Jobez, N. Timoney, C. Laplane, J. Etesses, A. Ferrier, P. Goldner, N. Gisin, and M. Afzelius, *Phys. Rev. A* **93**, 032327 (2016).
- [53] X. Ding, Y. He, Z. C. Duan, N. Gregersen, M. C. Chen, S. Unsleber, S. Maier, C. Schneider, M. Kamp, S. Höfling, C. Y. Lu, and J. W. Pan, *Phys. Rev. Lett.* **116**, 020401 (2016).
- [54] M. Sabooni, Q. Li, S. Kröll, and L. Rippe, *Phys. Rev. Lett.* **110**, 133604 (2013).
- [55] S. J. Yang, X. J. Wang, X. H. Bao, and J. W. Pan, *Nat. Photonics* **10**, 381 (2016).